



TITLE:

Experimental and numerical investigation of screening currents induced in a Bi-2223/Ag double pancake coil for space applications

AUTHOR(S):

Nagasaki, Y; Nakamura, T; Funaki, I; Ashida, Y; Yamakawa, H

CITATION:

Nagasaki, Y ...[et al]. Experimental and numerical investigation of screening currents induced in a Bi-2223/Ag double pancake coil for space applications. Superconductor Science and Technology 2014, 27(11): 115005.

ISSUE DATE:

2014-10-01

URL:

<http://hdl.handle.net/2433/200212>

RIGHT:

This is an author-created, un-copyedited version of an article accepted for publication in 'Superconductor Science and Technology'. The publisher is not responsible for any errors or omissions in this version of the manuscript or any version derived from it. The Version of Record is available online at <http://dx.doi.org/10.1088/0953-2048/27/11/115005>; This is not the published version. Please cite only the published version.; この論文は出版社版ではありません。引用の際には出版社版をご確認ご利用ください。

Experimental and numerical investigation of screening currents induced in Bi-2223/Ag double pancake coil for space applications

Experimental and numerical investigation of screening currents induced in Bi-2223/Ag double pancake coil for space applications

Y Nagasaki¹, T Nakamura², I Funaki³, Y Ashida¹ and H Yamakawa¹

¹ Research Institute of Sustainable Humanosphere, Kyoto University, Gokasho, Uji, Kyoto 611-0011, Japan

² Graduate School of Engineering, Kyoto University, Kyotodaigakukatsura, Nishikyo, Kyoto 615-8510, Japan

³ Institute of Space and Astronautical Science, Japan Aerospace Exploration Agency, Sagami-hara, Kanagawa 252-5210, Japan

E-mail: nagasaki@rish.kyoto-u.ac.jp

Abstract. We modelled screening currents (I_s) induced in high-temperature superconducting (HTS) coils to develop a method for the characterization and design of HTS magnets for space applications. The analysis made use of the so-called percolation depinning and flux creep models to describe the current density versus electric field in HTS tapes. We compared model results with experimental data obtained from a Bi-2223/Ag double pancake coil. The experimental residual magnetization due to I_s in the Bi-2223/Ag coil can be effectively modelled assuming an equivalent loop length of approximately 9 mm for I_s in the coil. The values calculated from the method quantitatively agreed with the results for various experimental conditions. We also successfully modelled the hysteresis of the magnetization due to I_s . These results demonstrate the validity of our model for I_s , which considers the effects of flux creep and smaller I_s loops in the multi-filamentary Bi-2223/Ag tape.

1. Introduction

There is much interest in developing high-temperature superconducting (HTS) coils for space applications [1], such as for a magnetic sail and electric propulsion. The space propulsion systems with HTS coils can have more thrust, since HTS coils weigh less, use less power and produce larger magnetic fields [2–9] than non-HTS coils. Since the acceleration of a magnetic sail is proportional to the magnetic moment/mass ratio of the installed coil, our purpose is to develop a light-weight HTS coil system with a higher magnetic moment, radiative and/or conductive cooling and light-weight DC/DC converters for the regulation of power supply in a spacecraft. A detailed explanation of the propulsion mechanism of a magnetic sail has been given by Yamakawa *et al* [5].

Space missions attach great importance to the reliability of instruments installed in a spacecraft. For HTS coils, great care is needed to avoid coil quench in space. To that end, we previously developed a thermo-electromagnetic field analysis method [10] that can

evaluate the thermal stability of the HTS coil. The analysis is based on the so-called percolation depinning model [11], which can quantitatively express the current density versus electric field in HTS tapes as a function of temperature and magnetic field vector.

However, one potential problem can arise from AC ripples in the output current of the DC/DC converter, which could generate screening currents (I_s) and AC losses in the HTS coil. Since a spacecraft cannot be equipped with any refrigerants, mostly because of mass considerations, the AC loss could become a serious problem for the reliability of an HTS coil. Moreover, the induced I_s could have large effects on the magnetic field distribution and current transport characteristics of the HTS coil itself [12–15]. These effects must be estimated to design optimal HTS coil systems for space missions. In addition, understanding I_s is highly important for terrestrial applications, e.g. magnetic resonance imaging, nuclear magnetic resonance imaging and cyclotrons, which require stable magnetic fields [12–15].

Experimental and numerical investigation of screening currents induced in Bi-2223/Ag double pancake coil for space applications

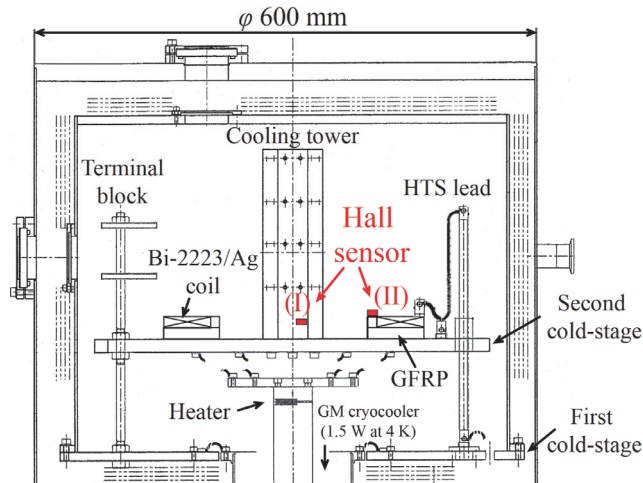


Figure 1. Schematic diagram of the inside of the vacuum chamber and setting of the Hall sensors for the experiments.

Table 1.
Specifications of the Bi-2223/Ag coil and tape.

Items	Scaled-down model coil [10]
Shape	Double pancake coil
Turn number	130 Layer \times 2 Stack
Inner diameter	0.200 m
Outer diameter	0.274 m
Tape width	4.2 mm
Tape thickness	0.28 mm
Tape length	200 m
Critical current I_{cmin} of the coil	200 A (50 K, E_{max} : 1 μ V/cm)

In this study, we investigated a Bi-2223/Ag coil, which is a candidate for magnetic sail spacecraft [10]. It has been reported that multi-filamentary Bi-2223/Ag tapes have superconducting connections (bridging) between neighbouring filaments [16–21]. The filament bridging can have effects on the loop length and inductance of I_s in the coil, and as a result, the AC loss and magnetic field distribution generated by the coil itself. Koyama *et al.* reported that due to the filament bridging, flux creep was a dominant factor for I_s induced in a Bi-2223/Ag coil [22]. To analyse the AC loss, magnetic field distribution and optimal design for the Bi-2223/Ag coil, it is essential to develop an analytical method that considers flux creep and understands how I_s is induced in the Bi-2223/Ag coil.

To evaluate the AC loss and magnetic field distribution of HTS coils accurately, we developed an analytical method to investigate I_s in a Bi-2223/Ag coil that considers the effect of flux creep. We validated the method by comparing calculated results to measured magnetic fields generated by I_s .

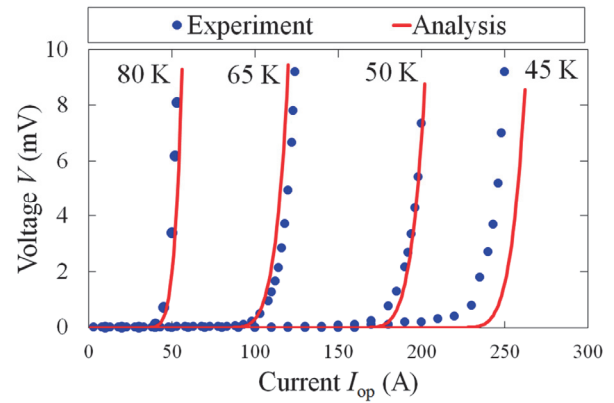


Figure 2. Experimental and analytical results of the current versus voltage characteristics of the Bi-2223/Ag scaled-down model coil at various temperatures, obtained in [10].

2. Experimental Method

2.1 Scaled-down model coil

As a scaled-down model for space applications, a double pancake coil was fabricated with a Bi-2223/Ag tape of 200 m length and was set at the second cold-stage in a conduction-cooled experimental system [10], as depicted in figure 1. The specifications of the coil are shown in table 1, and current, I_{op} , versus voltage, V , for the coil are shown in figure 2; we obtained these values in a previous study [10]. The minimum critical current, I_{cmin} , of the coil at 50 K was about 200 A (maximum electric field, E_{max} , in the coil was 1 μ V/cm at 200 A in self-field).

2.2 Experimental procedure

To investigate I_s induced in the coil during the coil excitation, we measured the axial magnetic fields generated by I_s with Hall sensors. The Hall sensors were installed at (I) the centre and (II) the top surface of the coil, as shown in figure 1. The residual magnetic fields due to I_s were obtained by subtracting the fields for the transport current (e.g. 1.17 mT/A at the centre of the coil, calculated by the integration of the Biot–Savart law without any screening currents) from the measured values. We measured the loop inductance and magnitude of I_s in the Bi-2223/Ag coil and compared them with the analytical results from the model.

To evaluate the inductance and loop length of I_s , the decay time constant, τ , was estimated. We measured the decay behaviour of the magnetic field due to I_s by pausing the increase of the operational current, I_{op} , for several times during the excitation of the coil up to 200 A. The measurements were conducted under various conditions: at different temperatures from 4 to 50 K and with different sweep rates from 40 to 80 A/min.

Experimental and numerical investigation of screening currents induced in Bi-2223/Ag double pancake coil for space applications

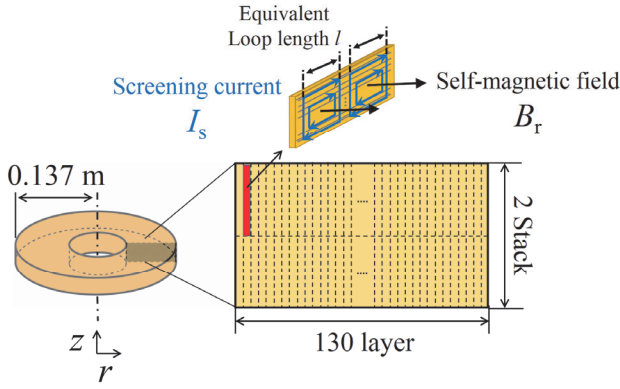


Figure 3. Analysis model of the Bi-2223/Ag double pancake coil. We assumed that all of the screening currents flowed with an equivalent loop length, l , in the Bi-2223/Ag coil.

To investigate the maximum ratio of the magnetic fields from I_s to those from the coil current, the hysteresis loops of the magnetization during charging and discharging of the coil were measured. The transport current was applied up and down to ± 200 A at 50 K with a 40 A/min sweep rate.

3. Analytical Model

We enhanced a thermo-electromagnetic field analysis method [10] by including the effects of flux flow and flux creep on I_s induced in HTS coils. Figure 3 shows the analysis model of the Bi-2223/Ag double pancake coil, whose features are described in table 1. I_s is induced by the temporal variation of the self-magnetic field, B_r , during the coil excitation and flow between filaments via the filament interconnections or silver sheath in the Bi-2223/Ag tape. We assumed I_s is induced by a single equivalent loop length, l , along the tape in the coil, as shown in figure 3. I_s was analysed using Faraday's law, the percolation depinning model, the flux creep model and the equivalent circuit of the HTS coil.

The electric field, E_s , induced by the temporal variation of the radial component of B_r linked with the operational current, I_{op} , and I_s is expressed as follows:

$$\nabla \times \mathbf{E}_s = -\frac{\partial \mathbf{B}_r}{\partial t}. \quad (1)$$

B_r at each time, t , is calculated using the Biot–Savart law.

Based on the percolation depinning model, the current

$$J = \begin{cases} J_{cm}(T, B_{eq}) + \left(\frac{m+1}{\rho_{FF}} E_{FF} J_0(T, B_{eq})^m \right)^{\frac{1}{m+1}} & \text{for } J_{cm} \geq 0, \\ -|J_{cm}(T, B_{eq})| + \left(\frac{m+1}{\rho_{FF}} E_{FF} J_0(T, B_{eq})^m + |J_{cm}(T, B_{eq})|^{m+1} \right)^{\frac{1}{m+1}} & \text{for } J_{cm} < 0 \end{cases} \quad (2)$$

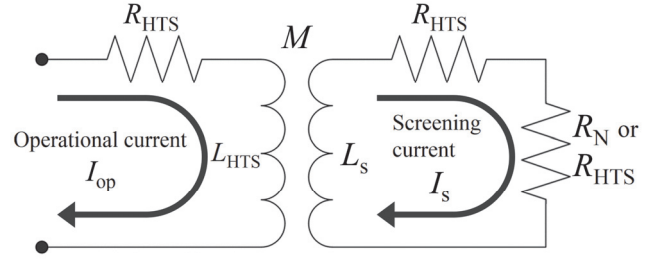


Figure 4. Equivalent circuit of the HTS coil. Both the operational transport current, I_{op} , and the screening current, I_s , in the HTS coil are considered.

density, J , versus the electric field, E , due to the flux flow relationship in HTS tapes can be described as a function of temperature, T , magnetic field and its applied angle [23–26] [equation (2)], where ρ_{FF} is the resistivity for uniform flux flow; J_{cm} , J_0 and m denote the minimum value, the scaling factor and the statistical parameter characterizing the shape of the local critical current density distribution, respectively, and B_{eq} denotes the equivalent perpendicular magnetic flux density, which describes the magnetic field anisotropy of HTS tapes [26].

Considering the influence of thermally activated vortex hopping, i.e. flux creep, the relationship between J and E , especially in a lower load factor region, can be written as follows [24]:

$$E_{FC} = \begin{cases} E_{c0} \exp\left[-\frac{U(j)}{kT}\right] \left[1 - \exp\left(-\frac{\pi U_0 j}{kT}\right)\right], & \text{for } J < J_c \\ E_{c0} \left[1 - \exp\left(-\frac{\pi U_0 j}{kT}\right)\right] & \text{for } J \geq J_c, \end{cases} \quad (3)$$

where $U(j) = U_0 [(1 - j^2)^{1/2} - j \cos^{-1} j]$, $E_{c0} = Ba_f v_0$ and $j = J/J_c$. a_f is the flux line lattice spacing, v_0 is the attempt frequency, U_0 is the height of the pinning potential for $j = 0$ and k is the Boltzmann constant. The total electric field from the flux flow and the flux creep can be calculated as the sum of the electric fields obtained from (2) and (3): $E(J) = E_{FF}(J) + E_{FC}(J)$ [27].

Figure 4 illustrates the equivalent circuit of the HTS coil. I_s can be obtained by satisfying the following equation:

Experimental and numerical investigation of screening currents induced in Bi-2223/Ag double pancake coil for space applications

$$\oint E_s ds = L_s \frac{dI_s}{dt} + R I_s, \quad (4)$$

where the subscript s and L_s , respectively, denote the loop element and the corresponding inductance for I_s as well as the resistance $R = R_{HTS} + (R_N \text{ or } R_{HTS})$. R_{HTS} is the equivalent resistance of the HTS tape based on the percolation depinning model (2) and the flux creep model (3). R_N is the resistance of the silver sheath [28] in cases where I_s flows across the silver matrix. We assume that the outermost current loops, shown in figure 3, flow via the filament interconnections with a length of l , and the inner current loops flow via the silver sheath in the Bi-2223/Ag tape. L_s is obtained by calculating \mathbf{B}_r from only I_s .

We compared the modelling results with the experimental ones assuming different values for loop length, l , for I_s to verify the validity of the analysis method and evaluate an equivalent l in the Bi-2223/Ag coil.

4. Results and Discussion

4.1 Decay behaviour of I_s in the Bi-2223/Ag coil

We first measured the decay behaviour of I_s with long-term operation of the coil. Figure 5 shows the experimental result of the temporal variation of the residual magnetization due to I_s , which was obtained by subtracting the magnetic field generated by the coil current from the measured one at Hall sensor (I). In this experiment, we increased I_{op} from 0 to 80 A at a rate of 40 A/min. At 80 A ($t = 0$ in figure 5), I_{op} was fixed and the decay of the magnetization was measured. A typical logarithmic decay in the magnetization is shown by a dashed line in figure 5. This result indicates that the decay behaviour of I_s in the Bi-2223/Ag coil is controlled by flux creep, as discussed by Koyama *et al.* [22] and Pust [29]. The result also suggests that much of I_s flows as persistent currents via the filament interconnections in the Bi-2223/Ag coil without any normal resistance [22]. Conversely, the rapid decay of the magnetization at $t < 3$ s in figure 5 suggests that some I_s in the Bi-2223/Ag coil flow across the silver sheath and rapidly disappear due to the resistance, R_N , of the silver sheath, as suggested by Koyama *et al.* [22]. Approximately 46% of the magnetic field generated by I_s rapidly diminished at $t < 3$ s. Because of this decay behaviour, we continued to consider both the flux creep and the silver sheath resistance in our analysis of I_s in the coil, as described in section 3.

As mentioned in section 2.2, we investigated the inductance and loop length, l , of I_s induced in the Bi-

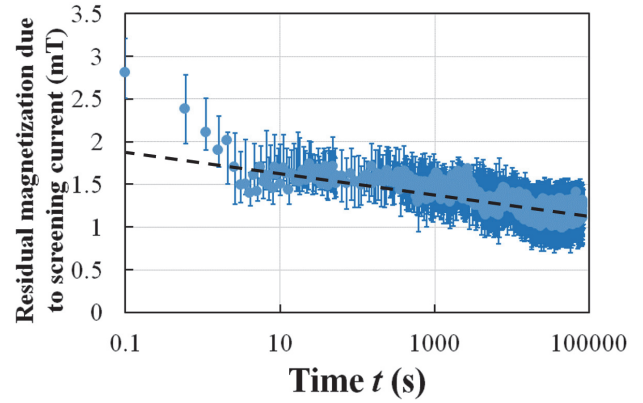


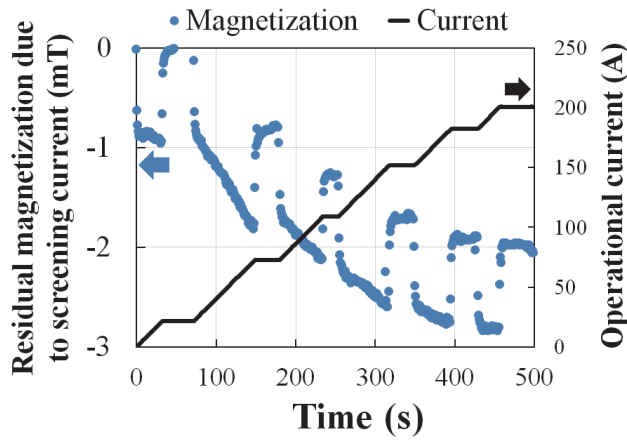
Figure 5. Semi-logarithmic plot of the temporal variation of the experimental residual magnetization at Hall sensor (I). I_{op} and T were 80 A and 50 K, respectively.

2223/Ag coil. We measured the decay time constant, τ , of the magnetic field generated by I_s due to the normal resistance, R_N , and fitted the model result to the measured one. The fitting parameter was l for I_s in the Bi-2223/Ag tape. The corresponding inductance, L_s , was obtained by calculating \mathbf{B}_r from only I_s of the loop itself and $\tau = L_s / R_N$.

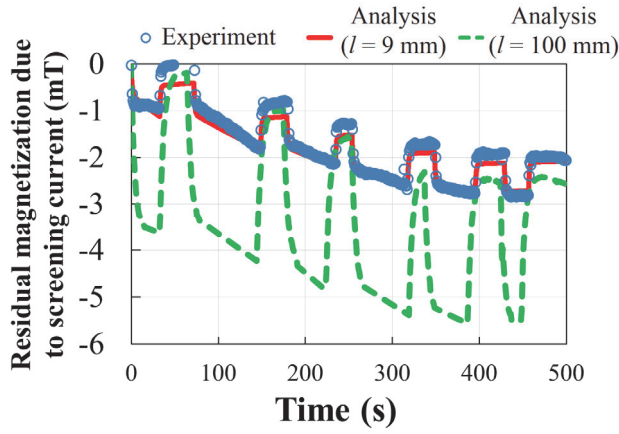
Figure 6(a) shows the temporal variation of the experimental residual magnetization due to I_s at Hall sensor (I). As previously mentioned in section 2.2 and as shown in figure 6(a), we intermittently halted the increase of I_{op} six times and investigated τ for the condition of no induced electric fields, \mathbf{E}_s , originating from I_{op} for various load factors, I_{op}/I_{cmin} , for the HTS coil. I_{op} was increased up to the minimum critical current, $I_{cmin} = 200$ A (when $E_{max} = 1.0 \mu\text{V}/\text{cm}$), with a fixed 40 A/min sweep rate and $T = 50$ K, and the magnetic field was measured every 0.5 s. The experimental results (solid circles) indicate that the magnetic field from I_s drastically decreased under constant current conditions with no induced electric field due to \mathbf{E}_s . In addition, the decay ratio and τ of the magnetic field slightly decreased with increasing load factor, i.e. increasing resistance of the HTS tape, R_{HTS} . The fact that this rapid decay was observed even at an extremely low load factor, i.e. at a no flux flow region, suggests that the decay is caused mainly by the influence of R_N and the flux creep, as in the case shown in figure 5. At $I_{op} = 20$ A, for example, τ of I_s is estimated to be approximately 0.9 s.

Figure 6(b) and table 2 depict the model fitting results assuming various values for l for I_s . The maximum value and decay time constant of the magnetic field for each l are shown in table 2. Considering the standard deviation of the measurements, the experimental results can be successfully modelled using $l = 9 \pm 3$ mm. This value of l is of the same order as the length of the filament bridging in a Bi-2223/Ag tape of approximately 5 mm,

Experimental and numerical investigation of screening currents induced in Bi-2223/Ag double pancake coil for space applications



(a) I_{op} and residual magnetization with time



(b) Analysis fitting result

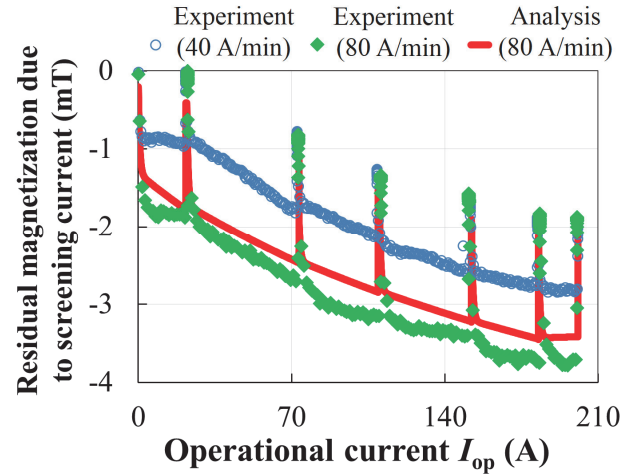
Figure 6. Temporal variations of (a) I_{op} and the magnetization generated by I_s at Hall sensor (I) and (b) fitting of the model for the magnetic field using two different values for l . $T = 50$ K, sweep rate = 40 A/min.

Table 2.

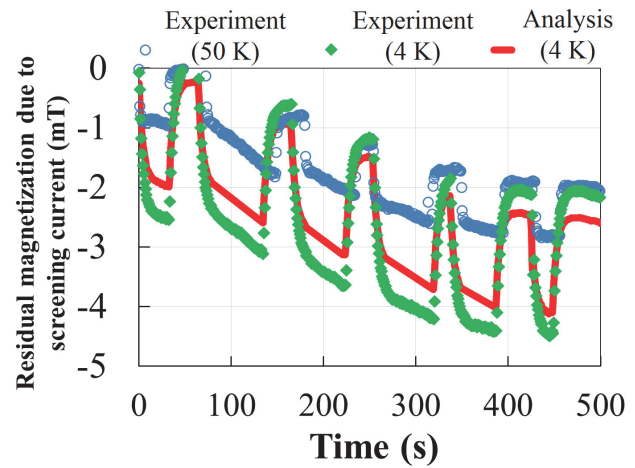
Experimental result and modelling for the magnetization due to I_s for different values of l . $T = 50$ K, sweep rate = 40 A/min.

	Maximum value of the magnetization	Decay time Constant τ
Experiment	2.8 mT	0.6–1.0 s
Analysis ($l = 5$ mm)	2.5 mT	0.4–0.6 s
Analysis ($l = 9$ mm)	2.7 mT	0.7–0.9 s
Analysis ($l = 50$ mm)	4.2 mT	2.5–3.2 s
Analysis ($l = 100$ mm)	5.5 mT	5.0–6.3 s

as suggested in a previous study [20]. This may imply



(a) For different sweep rates at $T = 50$ K



(b) For different T at sweep rate = 40 A/min

Figure 7. Temporal variations of the experimental and analytical results for the magnetic field generated by I_s at Hall sensor (I). The experimental and analytical conditions were (a) two different sweep rates of 40 and 80 A/min at $T = 50$ K and (b) two different temperatures, T , of 4 and 50 K for sweep rate 40 A/min.

that I_s flows through the filament bridging in the Bi-2223/Ag tape, as discussed for the results of figure 5. In addition, these results suggest that in Bi-2223/Ag tape, I_s is induced in smaller current loops compared to those in RE-system-coated conductors, such as GdBCO tapes.

The analytical results in figure 6(b) and table 2 also show the tendency of the smaller I_s loops to generate smaller magnetic fields. This result derives from the fact that in the case of a smaller loop, the maximum value of I_s becomes lower because of the smaller loop area and smaller E_s in (4). Consequently, I_s induced in Bi-2223/Ag tape with smaller loops due to the effect of the

Experimental and numerical investigation of screening currents induced in Bi-2223/Ag double pancake coil for space applications

filament bridging has less effect on the magnetic field distribution from the coil current than I_s in a coated conductor.

4.2 Effect of sweep rate and T

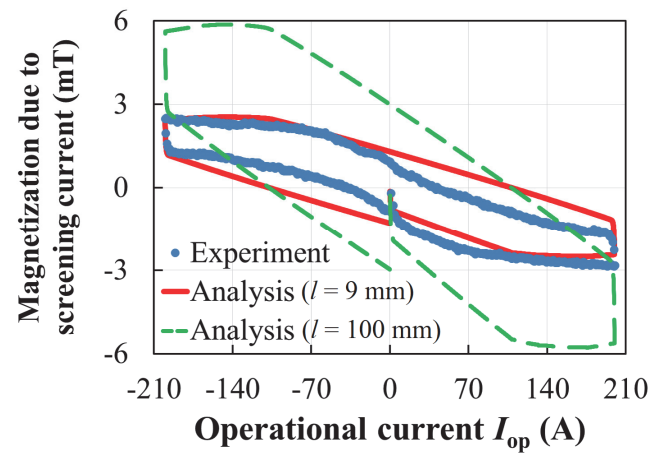
We also conducted experiments and analyses with varying sweep rates and T , examples of which are shown in figure 7. The horizontal axis is I_{op} in figure 7(a) and time in figure 7(b). The modelling for both figures assumes $l = 9$ mm. In figure 7(a), with increasing sweep rate, the temporal variation ratio of B_r and E_s increase, and as a result, the maximum value of the induced I_s increases according to (4). In the case of figure 7(b), with a decrease in T , R_N of the silver sheath decreases [28], and as a result, the maximum value and time constant, $\tau = L_s/R_N$, of I_s increases according to (4). These tendencies can be seen in the experimental results in figure 7 and can be modelled assuming $l = 9$ mm. This result indicates that the maximum value of I_s and its time constant in the Bi-2223/Ag coil are affected by the operational conditions of the coil and can be well described by the model.

4.3 Hysteresis effect of the magnetization due to I_s

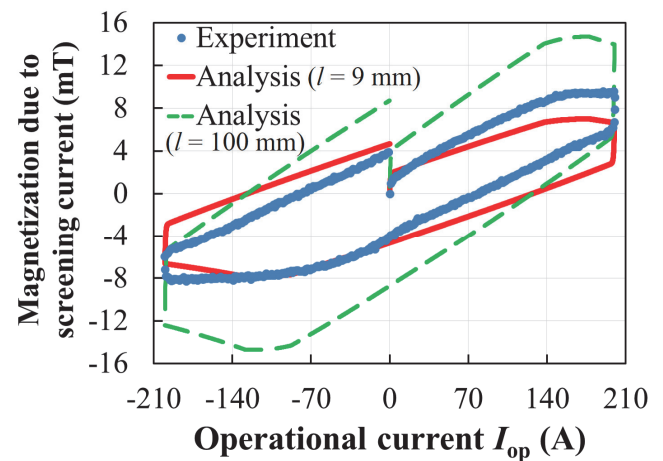
As mentioned in section 2.2, we measured the hysteresis of the magnetic field generated by I_s , and investigated the maximum ratio of the induced magnetic field to that of the coil current itself. Figure 8 illustrates the experimental data and the modelling of the magnetization due to I_s at Hall sensors (I) and (II). The measured data are the solid circles, and the polarity of the hysteresis loops is dependent on the position of the sensor relative to the coil [22]. I_s in the coil tends to saturate at specific values in a higher load factor region due to the increasing resistance of the HTS tape, R_{HTS} . Since the sweep rate of 40 A/min, which corresponds to 46 mT/min at Hall sensor (I), is much higher than τ due to the flux creep, which is of the order of nT/min– μ T/min, the decay effect due to flux creep is not detected in these hysteresis curves. The saturation values at the Hall sensors are (I) –2.85 mT and (II) 9.6 mT, which are only 1.2% and 1.8% of the magnetic field from I_{op} , respectively.

The modelling of the hysteresis loops are depicted in figure 8 as lines. We used $l = 9$ mm, as estimated in the previous section, and $l = 100$ mm for I_s . As shown in the figures, the modelling assuming $l = 9$ mm agrees well with the experimental data. These results also support the validity of the developed model, and suggest that l for I_s in the Bi-2223/Ag coil can be assumed as approximately 9 mm, which agrees well with the bridging length of the filament in the Bi-2223/Ag tape.

As also shown in figure 8, the saturation values of the



(a) Hall sensor (I)



(b) Hall sensor (II)

Figure 8. Experimental and analytical results for the hysteresis of the magnetization due to I_s in the coil; sweep rate = 40 A/min and $T = 50$ K.

magnetic field due to I_s greatly increase with the increasing loop length of I_s . This result indicates that the amount of the influence of I_s on the magnetic field generated by I_{op} depends on the loop length of I_s in the coil. Our model considering the loop length of I_s is surely helpful to estimate the effect of I_s on the magnetic field from I_{op} , which is directly related to the propulsive force of the magnetic sail. Our future work is to enhance the model in order to clarify the effect of the loop length of I_s on AC loss in HTS coils for space applications.

The developed model can also be applied to a coil made from RE-system-coated conductors. In this type of coil, a more complicated screening current will flow in the thin film superconducting area, and the influence of such a current upon the residual magnetic field will be a

Experimental and numerical investigation of screening currents induced in Bi-2223/Ag double pancake coil for space applications

focus of our future study.

5. Conclusion

To characterise and design optimal HTS coils for space missions, we developed a numerical analysis method based on the percolation depinning and the flux creep models, considering screening currents, I_s , induced in the coil. In this study, I_s induced in a Bi-2223/Ag double pancake coil was investigated and modelled. We measured the decay behaviour of the magnetic field due to I_s , and then modelled the results assuming an equivalent loop length, l , for I_s in the coil. The experimental and analytical results suggest that the decay behaviour of I_s in the Bi-2223/Ag tape was dominated by the silver sheath resistance and the flux creep, especially at a lower load factor. In addition, the experimental results under varying conditions could be quantitatively modelled assuming an equivalent l of approximately 9 mm for I_s in the coil. The good agreement between the measurements and the analyses proved the validity of our model, which considered the effects of the flux flow and flux creep on I_s induced in the HTS coil. The precise identification of the mechanism for the smaller loops of I_s and the effects of such loops on AC loss in the coil for space applications is our future work.

Acknowledgments

This work was supported in part by the engineering committee of the Institute of Space and Astronautical Science of the Japan Aerospace Exploration Agency and by a Grant-in-Aid for JSPS Fellows.

References

- [1] Nagasaki Y, Nakamura T, Funaki I, Ashida Y and Yamakawa H 2013 Conceptual design of YBCO coil with large magnetic moment for magnetic sail spacecraft *IEEE Trans. Appl. Supercond.* **23** 4603405
- [2] Zubrin R M and Andrews D G 1991 Magnetic sails and interplanetary travel *J. Spacecraft Rockets* **28** 197–203
- [3] Vulpetti G 1994 A critical-review on the viability of a space propulsion based on the solar-wind momentum flux *Acta Astron.* **32** 641–4
- [4] Winglee R M, Slough J, Ziembra T and Goodson A 2000 Mini-magnetospheric plasma propulsion: Tapping the energy of the solar wind for spacecraft propulsion *J. Geophys. Res.* **105** 21067–77
- [5] Yamakawa H, Funaki I, Nakayama Y, Fujita K, Ogawa H, Nonaka S, Kuninaka H, Sawai S, Nishida H, Asahi R, Otsu H and Nakashima H 2006 Magneto-plasma sail: An engineering satellite concept and its application for outer planet missions *Acta Astron.* **59** 777–84
- [6] Bruno C and Giucci S 2002 Cryogenic technology to improve electric thrusters *Acta Astron.* **51** 855–63
- [7] Bruno C and Casali D 2004 Superconducting materials applied to electric propulsion systems *J. Spacecraft Rockets* **41** 671–6
- [8] Rey C M, Hoffman W C, Chang-Diaz F R, Ilin A V, Petro A J, Winter D S, Mukai H and Schwenterly S W 2002 Design and fabrication of an HTS magnet for the VASIMR experiment *IEEE Trans. Appl. Supercond.* **12** 993–6
- [9] Wang Y, Li B, Zhang P and Wang S 2010 Magnet configuration and experimental analysis of helicon source for space magnetoplasma propulsion *IEEE Trans. Appl. Supercond.* **20** 993–6
- [10] Nagasaki Y, Nakamura T, Funaki I, Ashida Y and Yamakawa H 2013 Coupled-analysis of current transport performance and thermal behaviour of conduction-cooled Bi-2223/Ag double-pancake coil for magnetic sail spacecraft *Phys. C, Supercond.* **492** 96–102
- [11] Yamafuji K and Kiss T 1996 A new interpretation of the glass-liquid transition of pinned fluxoids in high-T-c superconductors *Phys. C, Supercond.* **258** 197–212
- [12] Hemmi T, Yanagi N, Seo K, Bansal G, Takahata K and Mito T 2007 Improvements of current decay behavior of HTS coils in persistent current operations *IEEE Trans. Appl. Supercond.* **17** 2422–5
- [13] Hahn S Y, Bascunan J, Kim W S, Bobrov E S, Lee H and Iwasa Y 2008 Field mapping, NMR lineshape, and screening currents induced field analyses for homogeneity improvement in LTS/HTS NMR magnets *IEEE Trans. Appl. Supercond.* **18** 856–9
- [14] Yanagisawa Y, Nakagome H, Uglietti D, Kiyoshi T, Hu R, Takematsu T, Takao T, Takahashi M and Maeda H 2010 Effect of YBCO-Coil Shape on the Screening Current-Induced Magnetic Field Intensity *IEEE Trans. Appl. Supercond.* **20** 744–7
- [15] Amemiya N and Akachi K 2008 Magnetic field generated by shielding current in high T c superconducting coils for NMR magnets *Supercon. Sci. Technol.* **21** 095001
- [16] Ashworth S P, Glowacki B A, Cizek M, Chesneau E C L and Haldar P 1997 Connectivity between filaments in BSCCO-2223 multi-filamentary tape *IEEE Trans. Appl. Supercond.* **7** 1662–5
- [17] Polak M, Majoros M, Kasztler A and Kirchmayr H 1999 Filament bridging and critical current density variation in the cross-section of multifilamentary Bi-2223/Ag tapes *IEEE Trans. Appl. Supercond.* **9** 2151–4
- [18] Bobyl A V, Shantsev D V, Johansen T H, Basiljevich M, Galperin Y M and Gaevski M E 2000 Temperature dependence of filament-coupling in Bi-2223 tapes: magnets-optical study *Supercond. Sci. Technol.* **13** 183–6
- [19] Bugoslavsky Y, Perkins G K, Buscemi P and Caplin A D 2001 Inhomogeneity of current distribution in multifilamentary BiSCCO-2223 tapes *Supercond. Sci. Technol.* **14** 245–51
- [20] Kvitkovic J and Polak M 2002 Remanent magnetisation in multifilamentary Bi-2223 tapes with filament bridging *Phys. C, Supercond.* **372** 1012–5
- [21] Demencic E, Usak P, Polak M, Piel H and Dhallo M 2006 Lateral critical current distribution and self-field profile of Bi-2223/Ag conductors: measurements and calculations *Supercon. Sci. Technol.* **19** 848–53
- [22] Koyama Y, Takao T, Yanagisawa Y, Nakagome H, Hamada M, Kiyoshi T, Takahashi M and Maeda H 2009 Towards beyond 1GHz NMR: Mechanism of the long-term drift of screening current-induced magnetic field in a Bi-2223 coil *Physica C: Superconductivity* **469** 694–701
- [23] Inoue M, Kiss T, Kuga T, Ishimaru M, Takeo M, Matsushita T, Iijima Y, Kakimoto K, Saitoh T, Awaji S, Watanabe K and Shiohara Y 2003 Estimation of E-J characteristics in a YBCO coated conductor at low temperature and very high magnetic field *Phys. C, Supercond.* **392-396** 1078–82
- [24] Kiss T, Inoue M, Kuga T, Ishimaru M, Egashira S, Irie S, Ohta T, Imamura K, Yasunaga M, Takeo M, Matsushita T, Iijima Y, Kakimoto K, Saitoh T, Awaji S, Watanabe K and Shiohara Y 2003 Critical current properties in HTS tapes *Phys. C, Supercond.* **392-396** 1053–62
- [25] Okamoto H, Kiss T, Nishimura S, Inoue M, Imamura K, Takeo M and Kanazawa M 2003 Prediction of E-J characteristics in Bi-2223/Ag tapes at low temperature and high magnetic field *IEEE Trans. Appl. Supercond.* **13** 3683–6
- [26] Nakamura T, Tsuchiya S, Fujio A, Hoshino T, Muta I and Yamaguchi M 2002 Angular dependence of E-J characteristics and dissipative properties in Bi-2223/Ag tape *Supercond. Sci. Technol.* **15** 230–5
- [27] Yamafuji K, Fujiyoshi T and Kiss T 2003 A theory of the thermal depinning transition in type-2 superconductors *Physica C: Superconductivity* **397** 132–50
- [28] Xiao L Y, Kiyoshi T, Ozaki O and Wada H 1999 Case study on quench evolution and passive protection of high T-c superconducting pancake coil *Cryogenics* **39** 293–8
- [29] Pust L 1990 Comparison between conventional flux creep in constant magnetic-field and the effect of creep on the shape of magnetic hysteresis loops in high-Tc superconductors *Supercond. Sci. Technol.* **3** 598–601